Master thesis
Local and non-local relaxation dynamics of hot electrons and holes analysed by time resolved linear photoemission

Florian Kühne

Faculty of physics, University Duisburg-Essen, Lotharstrasse 1, D-47057 Duisburg, Deutschland
Faculty of chemistry, University Duisburg-Essen, Universitätsstr.5, D-45141 Essen, Deutschland
21.08.2020

Abstract

This thesis utilised a time resolved linear photoemission (*tr*-LPE) measurement technique with a femtosecond resolution in a pump-probe scheme to analyse the transport mechanisms of laser excited non-equilibrium dynamics in a gold (Au) / iron (Fe) epitaxial heterostructure system. The motivation of the work was to observe ballistic propagation in Au / Fe layered systems. Previous efforts have shown, that the relaxation times increased with lower energies due to a bigger phase space. The concept is that at low enough energies for thin films the phase space would become large enough to observe ballistic propagation. The material system Au / Fe / MgO(001) was chosen, because of the epitaxial growth and the pristine interface conditions, as shown by Alekhin et al. [2] and Razdolski et al. [35]. Here Au is being probed as the propagation layer, where the transport occurs. And Fe acts as an excited electron injector layer, because of the good absorption, in the back side pump / front side probe and due to the shorter mean free path in Fe than in Au, as a sink for the excited electrons in case of front side pump / front side probe. The ~~described~~ dynamics are going to be studied by varying the thickness of the Au-layer. To differentiate the separate transport and relaxation contributions a previously developed back side pump / front side probe was used along with the usual front side pump / front side probe. The work of Beyazit et al. ~~utilised~~ *tr*-2PPE giving ~~good~~ insight into the non-equilibrium dynamics, but with ~~limited~~ access to electrons close to Fermi-level (E_F). The novelty of this work is that with *tr*-LPE the region from the Fermi-level to the pump photon energy can be probed above E_F, giving complementary data to previous experiments [9]. This is as well proof of ~~work~~ for the *tr*-LPE setup in back side pump configuration. Besides the extensively studied excited electron states, *tr*-LPE allows the observation of hole states below the Fermi-level and their relaxation back into thermal equilibrium through recombination. This work ~~will try~~ to further consolidate our understanding on how electron and hole relaxation dynamics interact and compete with the transport ~~into~~ the heterostructure. By analysis of the LPE signal as a function of pump-probe time delay an energy dependence for the peak intensity delay, like in Beyazit et al. [9], could be shown. In case of back side pump the analysis of electrons showed the same behaviour with lower energy electrons arriving later at the detector than the electrons with higher energy. This effect is thickness dependent indicating transport processes. Because the 'hot' electron dynamics around the Fermi-level are measured secondary electron dynamics are observed repopulating lower excited states and competing with the relaxation dynamic. Front side pump showed no delay in peak intensity, because the electrons did not have to propagate through the Au-layer. Laser calculations done in this work, show that for back side pump the excitation is predominantly in Fe with negligible excitation in Au, while in front side pump the Au-layer is homogeneously excited creating a gradient free non-equilibrium electron distribution. By determining

the energy density it was demonstrated that in back side pump more energy density reaches the Au surface with thinner gold layers, dissipating less incident energy during propagation, while in front side pump the energy density decreases with decreasing film thickness. Combination of the calculated incident laser absorption with the measured energy densities after propagation show, that in front side pump a bigger proportion of the actually absorbed energy reaches the detector compared to back side pump. For back side pump the efficiency of injection decreases with increasing film thickness. This loss of energy density is attributed to scattering events during propagation through the Au-layer. Through careful analysis of the energy resolved transients a spectral feature close to the Fermi-level,exclusive to back pump, could be identified. This peak is ascribed to d-band electrons in Fe. This work could measure depleted ground states as well as excited electrons, these electron holes below the Fermi-level exhibit a similar relaxation dynamic to the excited states, decaying on a timescale of 500 fs.

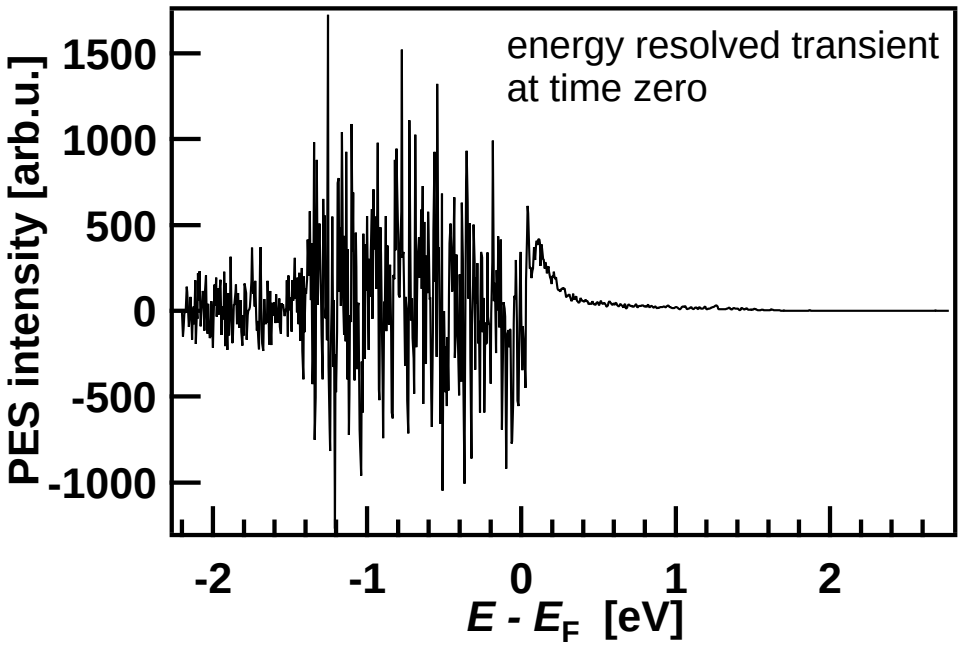

Figure 40: Energy dependent spectrum at time zero.

The next steps are checked by hand calculation as well. After storing all transients, a script is then run for analysis. First it sums the 5 meV bins up into 100 meV bins to make the data easier to be handled. In the future this limitation of energy resolution will be reduced by updating the code to work with the 5 meV bins.

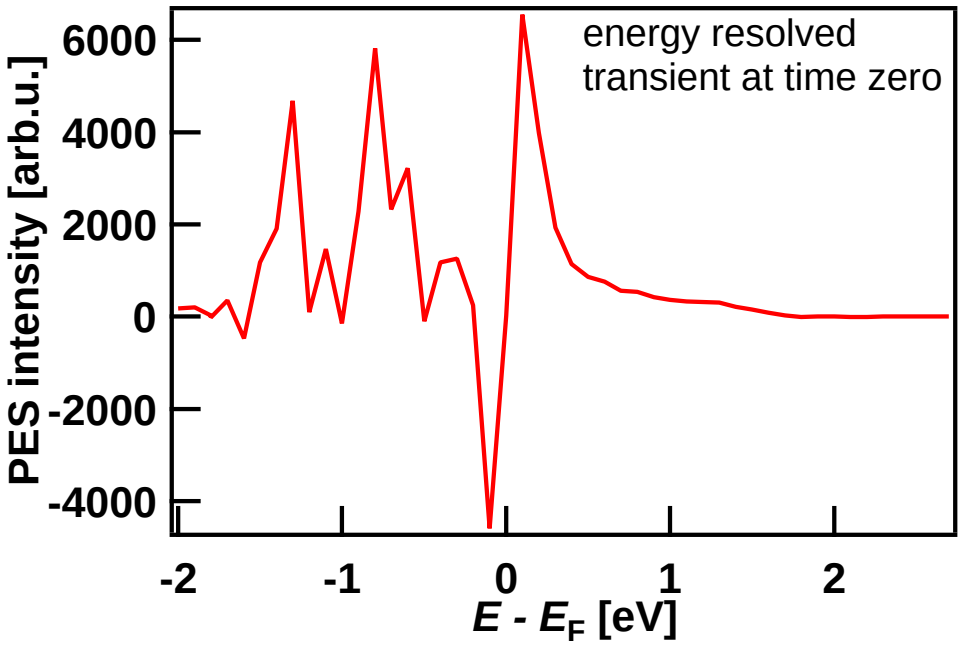

Figure 41: Energy dependent spectrum of time zero. Summed up in 100 meV bins for computational reasons.

To better describe the dynamics of the electrons and holes, the same analytic method as Lisowski et al. [26] used on *tr*-LPE measurements on Ru(001) was applied. First the relative number of electrons and holes around E_F was calculated [26].

$$n_{\pm} = \int_{0}^{\pm 0.3\,\mathrm{eV}} I(E,t)dE \tag{19}$$

With $n_{\pm}$ being the relative number or electrons and $I(E,t)$ the amount of events detected in the time of flight spectrometer with each count corresponding to a single electron hitting the detector. In order to analyse the various energy states and further find the limits of the data set the upper bound of the integral was varied from $E - E_F = 0$ to $\pm 0.6\,\mathrm{eV}$. Fig. 42 shows that most of the electron and hole dynamics do not appear at time zero, it takes a few tenth of femtoseconds to build up the intensity. Here all different integral bounds are shown to stress the point, that in the relative distribution most of the electrons and holes reside $\pm 200\,\mathrm{meV}$ around the Fermi-level. When multiplying the relative number of holes with -1 and omitting the higher energies, the symmetry of the electrons and holes become very apparent. The Fig. 43 features the relative number of electrons and holes integrated over the indicated upper bound.

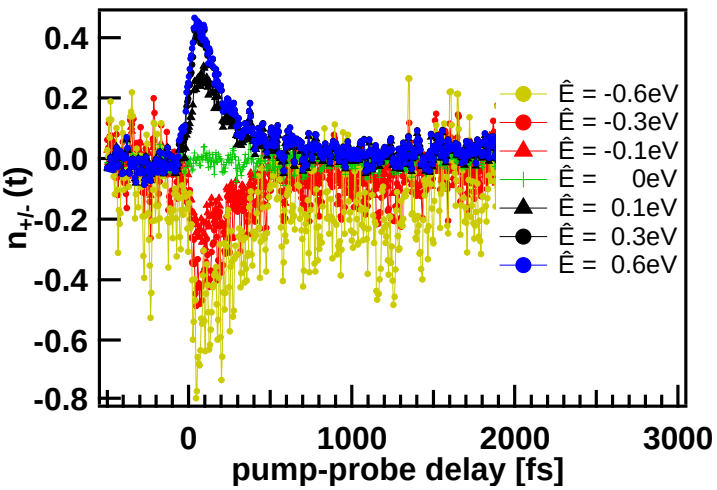

Figure 42: Electrons and holes for 5 nm Au / 7 nm Fe / MgO in back side pump configuration. Black and blue: Electrons, gold and red: Hole states.

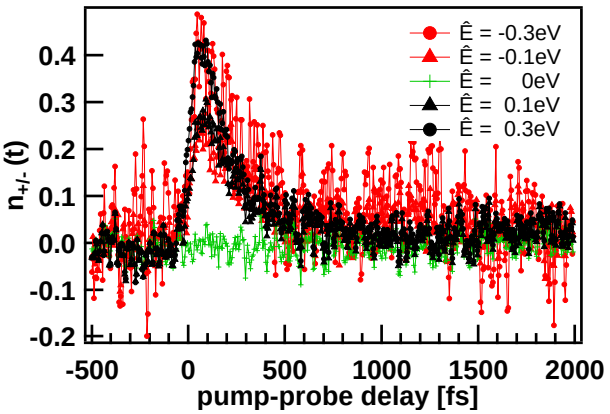

Figure 43: relative number of electrons and holes for 5 nm Au / 7 nm Fe / MgO in back side pump configuration. Black: Electrons, Red: Hole states

The integration is done in 100 meV bins and the Fermi-edge here is defined as the bin, where the excited electron signal and the reduction of signal by hole states cancel each other out to a zero baseline. If one sets the increased noise level of hole dynamics aside,the comparison reveals that the relative number of electrons and holes, displayed in Fig. 43, are almost identical.

The increased noise of the holes origins from the uncorrelated probe signal, which is five orders of magnitude bigger than the correlated signal. Both electrons and holes decay at the same rates. It is interesting to see, that despite integrating over an energy window three times the size, most electrons and holes are localised within the first 100 meV. This analysis was performed on the 5 nm Au / 7 nm Fe / MgO front

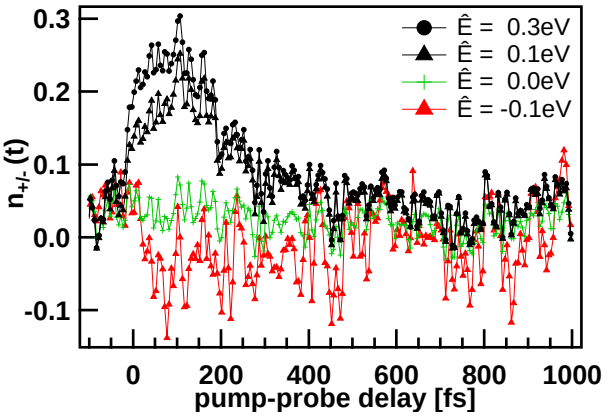

Figure 44: relative number of electrons and holes for 5 nm Au / 7 nm Fe / MgO in front side pump configuration. Black: Electrons, Red: Hole states, Green: Fermi-level.

pump / front side probe measurement as well. In front side pump / front side probe the identification of the reduction of signal is much less strait forward. The signal depletion is now also smaller and not of the same size as the corresponding electron energy. For 15 nm the back side pump measurement, the dynamic is slightly visible, but not distinguishable from background noise. In the rest of the measurements no depletion of ground state signal can be discerned.

Even if our approach is not sensitive enough, the excitation process has to create

the same number of holes like the observed excited electrons. Only 5 nm Au in both back and front side pump geometry showed observable depletion of ground states. Thicker Au films do not show these hole states, because they have a to low signal to noise ratio, as described in section 4.9. The relaxation of the electrons and hole states around E_{F} takes about 0.5 ps to decay. In FP the dynamics could be detected above the noise level up to the same time.
To now further analyse the electron dynamics, they get weighted by energy, as Lisowski et al. did [27].

4.7 Calculation of the Energy Density in the System

By weighting the energy of the electrons the information increases from a relative amount of excited electrons and holes to an amount of energy deposited in the probed area during a certain time step [26]. Lisowski has shown, that in order to relate the amount of energy deposited in a system with the intensity at the detector a proportionality factor needs to be incorporated [27].
The electronic energy of an electron distribution

$$N(E) = f(E,T) * D(E) \tag{20}$$

in a solid with the density of states $D(E)$ and the distribution function $f(E,T)$ is given by

$$U_{el} = \int_0^\infty N(E)\, E\, dE \quad \text{[27]}. \tag{21}$$

Lisowski then shows that the intensity I_{PES} being measured is related to the electronic escape depth λ_{PES} and a proportionality factor α. For Au the electronic escape depth λ_{PES} is estimated to be around 2 nm.

$$I_{PES}(E) = \frac{\alpha}{\lambda_{PES}} * f(E,T) * D(E) \tag{22}$$

Because $f(E,T)$ and $D(E)$ are unknown above the Fermi-level E_{F} the proportionality factor is calculated using a value $E_1 < E_{\mathrm{F}}$.

$$\alpha = \frac{I_{PES}(E_1)}{\lambda_{PES} * f(E_1,T) * D(E_1)} \tag{23}$$

Here $f(E_1,T)$ is assumed to be one, with E_1 far enough away from the Fermi-level and the density of states $D(E_1)$ taken from calculation [33]. Then eq. 21 and eq. 22 are combined and a factor two is added to account for the simultaneously created holes.

$$U(E,t) = \frac{2}{\alpha * \lambda_{PES}} \int_{E_F=0}^{1.6\,\mathrm{eV}} I(E,t)\ |E|\ dE \tag{24}$$

5 Discussion

5.1 Energy resolved transients

The energy resolved transients, showing the electron population distribution among the energies, for different times have demonstrated the repopulation of lower excited states by secondary electrons through the intersection of the intensity traces at energies $<$ 0.5 eV up to 250 fs. With higher energies depleting and lower excited states increasing at later times. The scattering of an excited electron with a ground state electron transfers about half the kinetic energy, creating two excited electrons with energies between 0 to 0.75 eV. This effect is less pronounced in front side pump. The behaviours of front and back side excitation are quite different, despite the pump and probe beams accessing similar areas, as shown in the laser calculations. Furthermore a spectral feature, exclusive to back side pumping, slightly above the Fermi-level E_F is observed. The peak might be a spectral feature of the Fe d-bands or a contribution of the interface proving the sensitivity of the *tr*-LPE method to the buried media. The spectral feature appears at time zero and a higher signal to noise ratio might help resolving the peak at later times.

The ~~energy density, except for the 15 nm Au back side pump measurement~~, is, in back side pump, much higher than in front side pump, because Fe absorbs a lot more of the pump beams energy. The laser calculations illustrated that for back side pump there is efficient injection, like in 30 nm Au back side pump about 90% of the incident light is absorbed by the Fe layer. In front side pump experiments the absorbed fluence increases with film thickness, while the injection efficiency decreases. The injection efficiency probably decreases, because it assumes absorption across the entire film thickness, while the 200 nm beam only probes the surface of the Au-layer with an estimated probing depth of around 5 nm. This provides an indication of the surface sensitivity of the method. By looking at the back side pump data it is apparent that most of the energy in back side pump gets lost during propagation, for 5 nm the detected energy density is 1.48 μJ/cm^2, 11.8% of the incident fluence. While at 30 nm the energy density drops to 0.6 μJ/cm^2, only a fraction of 1 % of the incident fluence, reaching the Au surface. The 15 nm back side pump measurement only detects 0.09 μJ/cm^2 of the 70 μJ/cm^2. This really low value is explained by a flawed measurement showing changes in the photoelectron yield of the detector over the duration of the measurement.

5.2 Relaxation times

The analysis of the energy density showed, that the electron dynamics behave differently if the pump beam arrives from the Fe back side or the Au front side. When back side pump / front side probe is employed the intensity builds up delayed, be-

Eigenständigkeitserklärung

Hiermit erkläre ich, dass ich diese Arbeit selbstständig verfasst, keine anderen als die angegebenen Quellen und Hilfsmittel benutzt, sowie Zitate kenntlich gemacht habe.

Duisburg, 21.08.2020

Florian Kühne